PI3K therapy reprograms mitochondrial trafficking to fuel tumor cell invasion

M. Cecilia Caino[a,b], Jagadish C. Ghosh[a,b], Young Chan Chae[a,b], Valentina Vaira[c,d], Dayana B. Rivadeneira[a,b], Alice Faversani[d], Paolo Rampini[e], Andrew V. Kossenkov[f], Katherine M. Aird[g], Rugang Zhang[g], Marie R. Webster[b], Ashani T. Weeraratna[b], Silvano Bosari[d,h], Lucia R. Languino[a,i], and Dario C. Altieri[a,b,1]

[a]Prostate Cancer Discovery and Development Program, The Wistar Institute, Philadelphia, PA 19104; [b]Tumor Microenvironment and Metastasis Program, The Wistar Institute, Philadelphia, PA 19104; [c]Istituto Nazionale Genetica Molecolare "Romeo ed Enrica Invernizzi," Milan 20122, Italy; [d]Division of Pathology, Fondazione Istituto di Ricovero e Cura a Carattere Scientifico (IRCCS) Ca' Granda Ospedale Maggiore Policlinico, Milan 20122, Italy; [e]Division of Neurosurgery, Fondazione IRCCS Ca' Granda Ospedale Maggiore Policlinico, Milan 20122, Italy; [f]Center for Systems and Computational Biology, The Wistar Institute, Philadelphia, PA 19104; [g]Gene Expression and Regulation Program, The Wistar Institute, Philadelphia, PA 19104; [h]Department of Pathophysiology and Organ Transplant, University of Milan, Milan 20122, Italy; and [i]Department of Cancer Biology, Kimmel Cancer Center, Thomas Jefferson University, Philadelphia, PA 19107

Edited by Vincent T. Marchesi, Yale University School of Medicine, New Haven, CT, and approved May 26, 2015 (received for review January 13, 2015)

Molecular therapies are hallmarks of "personalized" medicine, but how tumors adapt to these agents is not well-understood. Here we show that small-molecule inhibitors of phosphatidylinositol 3-kinase (PI3K) currently in the clinic induce global transcriptional reprogramming in tumors, with activation of growth factor receptors, (re)phosphorylation of Akt and mammalian target of rapamycin (mTOR), and increased tumor cell motility and invasion. This response involves redistribution of energetically active mitochondria to the cortical cytoskeleton, where they support membrane dynamics, turnover of focal adhesion complexes, and random cell motility. Blocking oxidative phosphorylation prevents adaptive mitochondrial trafficking, impairs membrane dynamics, and suppresses tumor cell invasion. Therefore, "spatiotemporal" mitochondrial respiration adaptively induced by PI3K therapy fuels tumor cell invasion, and may provide an important antimetastatic target.

mitochondria | molecular therapy | cytoskeleton | PI3K | cell invasion

The phosphatidylinositol 3-kinase (PI3K) is a universal tumor driver (1) that integrates growth factor signaling with downstream circuitries of cell proliferation, metabolism, and survival (2). Exploited in nearly every human tumor, including through acquisition of activating mutations (3), PI3K signaling is an important therapeutic target, and several small-molecule antagonists of this pathway have entered clinical testing (4). However, the patient response to these agents has been inferior to expectations (5), dampened by drug resistance (6) and potentially other mechanisms of adaptation by the tumor (7).

In this context, there is evidence that therapeutic targeting of PI3K promotes tumor adaptation, paradoxically reactivating protein kinase B (PKB/Akt) in treated cells (8) and reprogramming mitochondrial functions in bioenergetics and apoptosis resistance (9). How these changes affect tumor traits, however, is unclear. Against the backdrop of a ubiquitous "Warburg effect" (10), where tumors switch from cellular respiration to aerobic glycolysis, a role of mitochondria in cancer has not been clearly defined (11) and at times has been proposed as that of a tumor suppressor (12).

In this study, we examined the impact of mitochondrial reprogramming induced by PI3K therapy on mechanisms of tumor progression.

Results

PI3K Therapy Reactivates Akt and Mammalian Target of Rapamycin Signaling. Treatment of patient-derived glioblastoma (GBM) organotypic cultures (13) with PX-866, an irreversible pan-PI3K antagonist currently in the clinic (4), caused transcriptional up-regulation of multiple growth factor receptor pathways (Fig. 1*A*). This was associated with widespread phosphorylation, namely activation of the GBM kinome in primary organotypic cultures (Fig. 1*B* and Table S1) as well as GBM LN229 cells (Fig. S1*A*). Consistent with previous observations (8), structurally diverse small-molecule PI3K antagonists induced robust (re)phosphorylation of Akt1 (S473) and Akt2 (S474) in tumor cells (Fig. 1*C* and Fig. S1*B*), as well as phosphorylation of downstream mammalian target of rapamycin (mTOR) and its effectors, 70S6K and 4EBP1 (Fig. 1*D* and Fig. S1*C*). Similar results were obtained in primary 3D GBM neurospheres, where PI3K therapy strongly induced Akt (Fig. 1*E*) and mTOR (Fig. 1*F*) phosphorylation. By transcriptome analysis, PI3K antagonists up-regulated two main gene networks of protection from apoptosis (9) and increased cell motility (Fig. 1*G*) in treated tumors.

Increased Tumor Cell Motility Mediated by PI3K Therapy. Consistent with these data, PI3K inhibitors vigorously stimulated tumor cell invasion across Matrigel-coated Transwell inserts (Fig. 2 *A* and *B* and Fig. S1 *D* and *E*) and in 3D tumor spheroids (Fig. 2 *A* and *B*). Tumor cell proliferation was not significantly affected (Fig. S1*F*) (9). In addition, PI3K therapy dose-dependently increased the number and size of 3D GBM neurospheres (Fig. 2*C* and Fig. S1 *G* and *H*).

Significance

Despite the promise of personalized cancer medicine, most molecular therapies produce only modest and short-lived patient gains. In addition to drug resistance, it is also possible that tumors adaptively reprogram their signaling pathways to evade therapy-induced "stress" and, in the process, acquire more aggressive disease traits. We show here that small-molecule inhibitors of PI3K, a cancer node and important therapeutic target, induce transcriptional and signaling reprogramming in tumors. This involves the trafficking of energetically active mitochondria to subcellular sites of cell motility, where they provide a potent, "regional" energy source to support tumor cell invasion. Although this response may paradoxically increase the risk of metastasis during PI3K therapy, targeting mitochondrial reprogramming is feasible, and could provide a novel therapeutic strategy.

Author contributions: M.C.C. and D.C.A. designed research; M.C.C., J.C.G., Y.C.C., V.V., D.B.R., A.F., K.M.A., R.Z., M.R.W., and A.T.W. performed research; P.R. contributed new reagents/analytic tools; P.R. provided primary, patient-derived glioblastoma samples; K.M.A. and R.Z. performed and analyzed quiescence studies in tumor cells; M.R.W. and A.T.W. performed and analyzed 3D cell invasion assays; M.C.C., A.V.K., S.B., L.R.L., and D.C.A. analyzed data; and M.C.C., J.C.G., and D.C.A. wrote the paper.

The authors declare no conflict of interest.

This article is a PNAS Direct Submission.

[1]To whom correspondence should be addressed. Email: daltieri@wistar.org.

This article contains supporting information online at www.pnas.org/lookup/suppl/doi:10.1073/pnas.1500722112/-/DCSupplemental.

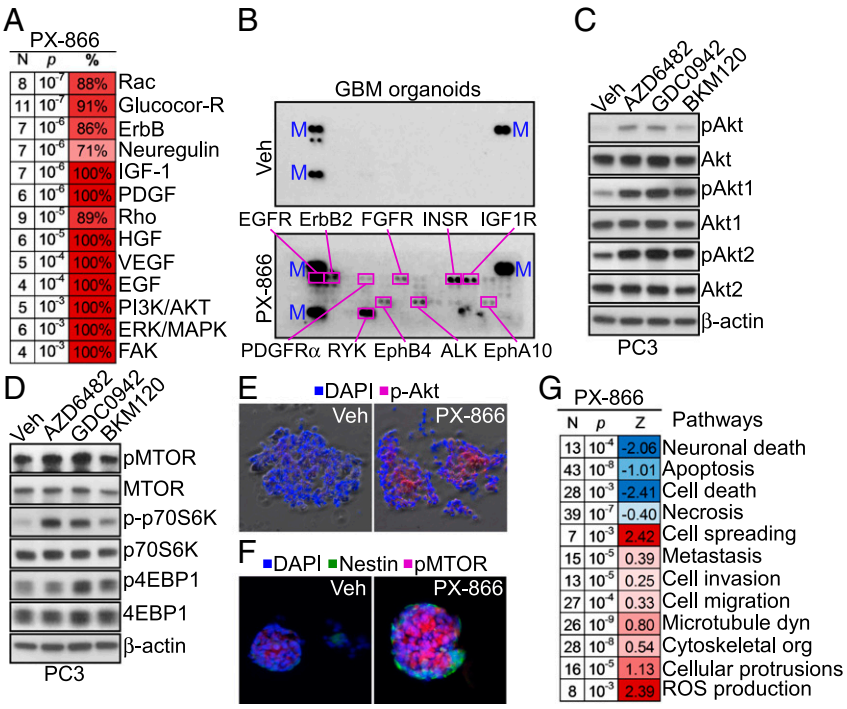

Fig. 1. PI3K therapy-induced tumor transcriptional reprogramming. (*A*) Heat map of changes in kinome functions in patient-derived GBM organotypic cultures treated with vehicle or PX-866 (10 μM for 48 h). *N*, number of genes; %, percentage of genes changed for any given function. (*B*) Extracts from GBM organotypic cultures treated with vehicle (Veh) or PX-866 (10 μM for 48 h) were incubated with a human phospho-RTK array followed by enhanced chemiluminescence detection. The position and identity of phosphorylated proteins are indicated. M, markers. (*C* and *D*) PC3 cells were treated with vehicle or the indicated PI3K inhibitors for 48 h and analyzed for changes in Akt (*C*) or mTOR (*D*) activation by Western blotting. p, phosphorylated. (*E* and *F*) Primary GBM spheroids treated with vehicle or 10 μM PX-866 for 48 h were imaged by phase-contrast and fluorescence microscopy for phosphorylated Akt (Ser473) (*E*) or mTOR (Ser2448) (*F*). DNA was counterstained with DAPI. Nestin is a GBM marker. (*G*) Heat map of changes in kinome pathways in GBM organotypic cultures treated with vehicle or PX-866 (10 μM) for 48 h. *N*, number of changed genes; Z, z score of the estimated function state: positive (red) indicates overall function is likely increased; negative (blue) indicates it is decreased.

To understand the basis of this cell invasion response, we next quantified the dynamics of membrane lamellipodia, which are required for cell motility, by single-cell stroboscopic microscopy (SACED, Fig. S2*A*) (14, 15). PI3K antagonists strongly stimulated lamellipodia dynamics (Fig. S2*B*), increasing the size (Fig. 2*D*, *Top* and Fig. S2*C*) and time of persistence (Fig. 2*D*, *Bottom* and Fig. S2*D*) of membrane ruffles compared with control cultures. Ruffle frequency was not affected (Fig. S2*E*). In addition, PI3K therapy changed the topography of membrane ruffles in tumor cells, with appearance of dynamic ruffles at lagging areas of the plasma membrane (Fig. 2*E* and Movie S1), potentially associated with random cell motility (16). These lateral ruffles were larger and persisted for a longer time in response to PI3K therapy compared with untreated cells (Fig. 2*F*), where membrane ruffles were instead polarized at the leading edge of migration (Fig. 2*E*). Consistent with these findings, PI3K antagonists strongly stimulated 2D tumor chemotaxis (Fig. S3*A*), extending the radius of cell migration (Fig. S3*B*) and promoting random, as opposed to directional, cell movements (Fig. 2*G*). Tumor cell movement in response to PI3K therapy proceeded at faster speed (Fig. S3*C*) and for longer distances (Fig. S3*D*) compared with untreated cultures.

Mitochondrial Repositioning to the Cortical Cytoskeleton Supports Adaptive Tumor Cell Invasion. When analyzed by fluorescence microscopy, PI3K therapy induced profound changes in the morphology and distribution of mitochondria. Whereas untreated cells exhibited mitochondria that were polarized and mostly clustered around the nucleus (Fig. S4 *A* and *B*), PI3K inhibitors caused the appearance of elongated mitochondria (Fig. S4*A*) that "infiltrated" the cortical cytoskeleton of tumor cells, localizing in proximity of membrane protrusions implicated in cell motility (Fig. 3 *A*–*C* and Fig. S4*B*). This was a general response of heterogeneous tumor cell types, as lung adenocarcinoma A549 or glioblastoma LN229 cells comparably repositioned mitochondria to the cortical cytoskeleton in response to PI3K therapy (Fig. 3*D* and Fig. S4*C*). Mitochondria are highly dynamic organelles, regulated by cycles of fusion and fission (17). Small interfering RNA (siRNA) knockdown of effectors of mitochondrial fusion, mitofusin (MFN)1 or MFN2 (Fig. S4*D*), did not affect cell viability (Fig. S4*E*) or ATP production (Fig. S4*F*) in tumor cells. Under these conditions, MFN1 silencing suppressed mitochondrial trafficking to the cortical cytoskeleton (Fig. 3*E* and Fig. S4 *G* and *H*) as well as tumor cell invasion (Fig. 3*F*) induced by PI3K therapy. The combination of MFN2 knockdown plus PI3K inhibition induced extensive loss of cell viability (MFN1 siRNA+PX-866, $2.7 \pm 0.05 \times 10^5$ cells; MFN2 siRNA+PX-866, $0.16 \pm 0.13 \times 10^5$ cells; $P = 0.0047$), thus preventing additional studies of mitochondrial relocalization or tumor cell invasion.

Requirements of Mitochondrial Regulation of Tumor Cell Invasion. A prerequisite of cell movements is the timely assembly/disassembly of focal adhesion (FA) complexes (14), and a role of mitochondrial trafficking in this process was next investigated. Mitochondria repositioned to the cortical cytoskeleton in response to PI3K antagonists colocalized with phosphorylated (Y925) focal adhesion kinase (FAK) (Fig. 3*G* and Fig. S5*A*). This was associated with increased FAK phosphorylation (Y925) compared with control cultures (Fig. S5*B*), suggesting deregulation of FA dynamics (18). By time-lapse video microscopy (Fig. S5*C*), PI3K

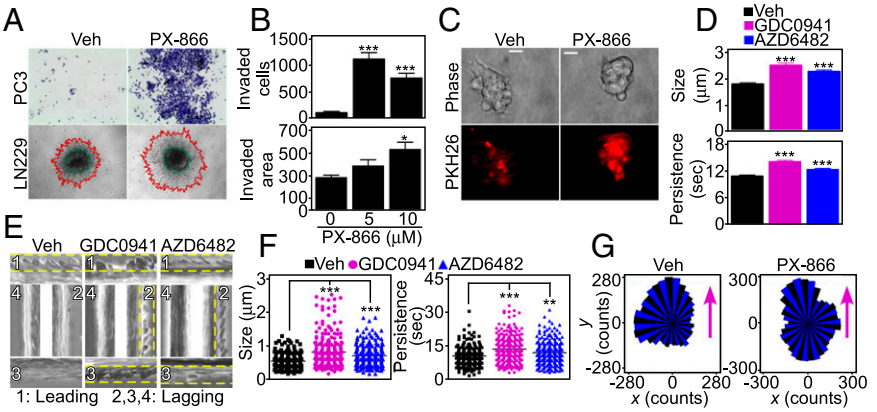

Fig. 2. PI3K therapy induces adaptive tumor cell motility and invasion. (*A*) Tumor cells treated with vehicle or 10 μM PX-866 for 48 h were analyzed for invasion across Matrigel-coated Transwell inserts (*Top*) or in 3D spheroids (*Bottom*). Red, invasive edge; green, core. Representative images. Magnification, 10×. (*B*) PC3 (*Top*) or LN229 (*Bottom*) cells were treated with the indicated increasing concentrations of PX-866 and quantified for invasion across Matrigel (*Top*) or in 3D spheroids (*Bottom*). The distance between the core and edge of 3D spheroids was determined. Mean ± SEM of replicates from a representative experiment. $*P = 0.02$; $***P < 0.0001$. (*C*) Patient-derived GBM spheroids were treated with vehicle or PX-866 (0–10 μM) for 48 h and analyzed by phase-contrast (*Top*) or fluorescence microscopy (*Bottom*). The vital dye PKH26 was used to counterstain live GBM neurospheres. (Scale bar, 20 μm.) (*D*) Membrane ruffling was quantified in PC3 cells treated with vehicle or PI3K inhibitors for 48 h by SACED microscopy. Average values from at least 330 ruffles per treatment are shown for ruffle size (*Top*) and time of ruffle persistence (*Bottom*). Mean ± SEM ($n = 15$). $***P < 0.0001$. (*E*) Representative stroboscopic images from time-lapse video microscopy of PC3 cells treated with vehicle or PI3K inhibitors. Four SACED regions corresponding to the top (1), right (2), bottom (3), and left (4) of each cell are shown. The ruffling activity (broken yellow lines) is restricted to one main region (1) on the vehicle cell but is distributed equally between three regions (1–3) on cells treated with PI3K inhibitors. See also Movie S1. (*F*) PC3 cells were treated with vehicle or PI3K inhibitors, and membrane dynamics at lagging areas were quantified. Ruffle size (*Left*) or time of ruffle persistence (*Right*) from at least 205 individual lagging ruffles are shown. Mean ± SEM ($n = 15$). $**P = 0.0047$; $***P < 0.0001$. (*G*) PC3 cells were treated with vehicle or PX-866 for 48 h and quantified for directional versus random cell migration by time-lapse video microscopy (8 h). Rose plots show the distribution of cells migrating along each position interval (range interval 10°, internal angle 60°). Arrows indicate the direction of chemotactic gradient.

therapy profoundly affected FA dynamics (Fig. 3*H* and Movie S2), increasing both the assembly and decay of FA complexes (Fig. S5*D*) and their turnover rate (Fig. S5*E*). In contrast, PI3K inhibition reduced the number of stable FA complexes (Fig. S5*F*).

Mitochondria are a primary source of reactive oxygen species (ROS), and these moieties have been implicated in tumor cell motility. PI3K antagonists increased the production of mitochondrial superoxide in tumor cells compared with untreated cultures (Fig. S6 *A* and *B*), and this response was abolished by a mitochondrial-targeted ROS scavenger, mitoTEMPO (Fig. S6*C*). In contrast, ROS scavenging with mitoTEMPO did not affect mitochondrial repositioning to the cortical cytoskeleton (Fig. 4*A* and Fig. S6 *D* and *E*) or tumor cell invasion (Fig. 4*B*) mediated by PI3K inhibitors. Increasing concentrations of the pan-antioxidant *N*-acetyl cysteine (NAC) had no effect on PI3K therapy-mediated tumor cell invasion (Fig. S6*F*). The increase in basal cell motility in the presence of antioxidants may reflect release of ROS-regulated inhibitory mechanisms of mitochondrial trafficking.

Role of Bioenergetics in Mitochondrial Trafficking and Tumor Cell Invasion. Next, we asked whether mitochondrial bioenergetics was important for this pathway, and generated LN229 cells devoid of oxidative phosphorylation (ρ0 cells). Chemoattractant stimulation of respiration-competent LN229 cells induced repositioning of mitochondria to the cortical cytoskeleton (Fig. S7*A*) that colocalized with paxillin$^+$ FA complexes (Fig. S7*B*). In contrast, respiration-deficient LN229 ρ0 cells failed to reposition mitochondria to the cortical cytoskeleton (Fig. 4*C*). This absence of mitochondria proximal to FA complexes (Fig. 4*D*) was associated with loss of FA dynamics (Fig. S7 *C* and *D* and Movie S3) and suppression of tumor cell invasion across Matrigel-containing inserts (Fig. 4*E* and Fig. S7*E*).

As an independent approach, we treated tumor cells with Gamitrinib, a mitochondrial-targeted small-molecule Hsp90 inhibitor that induces misfolding and degradation of the oxidative phosphorylation complex II subunit SDHB (19). Nontoxic concentrations of Gamitrinib abolished the trafficking of mitochondria to pFAK-containing FA complexes in response to PI3K antagonists (Fig. 4 *F* and *G*) and preserved a polarized and perinuclear mitochondrial distribution (Fig. S8*A*). Consistent with these findings, Gamitrinib abolished the increase in tumor cell invasion (Fig. 4*H*) and the expansion of primary GBM neurospheres (Fig. S8 *B* and *C*) mediated by PI3K antagonists. To validate these findings, we next silenced the expression of TRAP-1 (Fig. S8*D*), a mitochondrial Hsp90-like chaperone targeted by Gamitrinib and implicated in complex II stability (19). TRAP-1 silencing in vehicle-treated cells did not affect mitochondrial localization (Fig. S8*E*, *Left*). In contrast, knockdown of TRAP-1 abolished mitochondrial trafficking to the cortical cytoskeleton in the presence of PI3K antagonists, increasing the fraction of polarized and perinuclear organelles in these cells (Fig. S8*E*, *Right*). Finally, treatment with small-molecule inhibitors of mitochondrial complex I (Rotenone), complex III (Antimycin A), or complex V (Oligomycin) or a mitochondrial uncoupler (carbonyl cyanide *m*-chlorophenyl hydrazine; CCCP) inhibited mitochondrial repositioning to the cortical cytoskeleton (Fig. S8*F*) and tumor cell invasion (Fig. 4*I*) in the presence of PI3K therapy.

To begin elucidating the signaling requirements of adaptive mitochondrial trafficking and tumor cell invasion, we next targeted the PI3K–Akt–mTOR axis, which becomes reactivated in response to PI3K therapy (8, 9). Knockdown of Akt1 or Akt2 (Fig. S9*A*), mTOR (Fig. S9*B*), or FAK (Fig. S9*C*) independently prevented the repositioning of mitochondria to the cortical cytoskeleton (Fig. 4 *J* and *K* and Fig. S9*D*) and suppressed tumor cell invasion (Fig. 4*L* and Fig. S9*G*) induced by PI3K antagonists. In contrast, knockdown of these molecules in the absence of PI3K inhibition had no effect on mitochondrial trafficking (Fig. S9*E*) or organelle morphology (Fig. S9*F*).

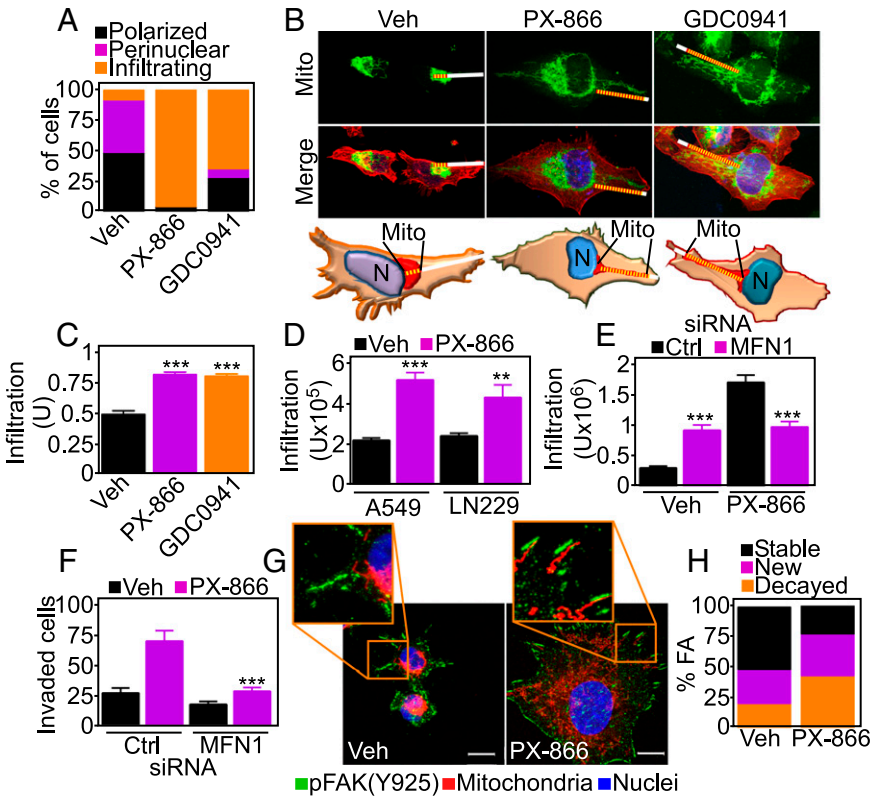

Fig. 3. Mitochondria fuel focal adhesion dynamics. (*A*) PC3 cells treated with vehicle or PI3K inhibitors for 48 h were stained with MitoTracker Red, phalloidin Alexa488, and DAPI, and full cell stacks were used to generate 3D max projection images that were scored for mitochondrial morphology (polarized, perinuclear, infiltrating). (*B*) Representative confocal 3D max projection images of PC3 cells treated with vehicle or the indicated PI3K inhibitors and stained as in *A*. (*Bottom*) Models for quantification of mitochondrial trafficking. Mito, mitochondria. White lines indicate the distance from nuclei to the cell border. Yellow lines indicate the length of mitochondrial infiltration into membrane lamellipodia. Magnification, 63×. (*C*) PC3 cells treated with vehicle or the indicated PI3K inhibitors were labeled as in *A* and quantified for mitochondrial infiltration into lamellipodia. At least 18 cells were analyzed at two independent lamellipodia, and data were normalized to total lamellipodia length. Mean ± SEM ($n = 36$). ***$P < 0.0001$. (*D*) Lung adenocarcinoma A549 or glioblastoma LN229 cells were labeled as in *A* and scored for mitochondrial infiltration into membrane lamellipodia by fluorescence microscopy. Mean ± SEM. **$P = 0.0056$; ***$P < 0.0001$. (*E*) PC3 cells were transfected with control (Ctrl) or MFN1-directed siRNA, labeled as in *A*, and quantified for mitochondrial infiltration in the cortical cytoskeleton in the presence of vehicle or PX-866. Mean ± SEM. ***$P < 0.0001$. (*F*) PC3 cells transfected with control or MFN1-directed siRNA were treated with vehicle or PX-866 and analyzed for Matrigel invasion after 48 h. Mean ± SEM. ***$P = 0.0002$. (*G*) PC3 cells treated with vehicle or PI3K inhibitors for 48 h were replated onto fibronectin-coated slides for 5 h and labeled with an antibody to phosphorylated FAK (pY925) Alexa488, MitoTracker Red, and DAPI. Representative 1-μm extended-focus confocal images with localization of mitochondria near FA complexes are shown. Magnification, 63×. (Scale bar, 10 μm.) (*H*) PC3 cells expressing Talin-GFP to label FA were treated as indicated and quantified for decay, formation, and stability of FA complexes per cell over 78 min; $n = 631$. See also Movie S2.

Discussion

In this study, we have shown that small-molecule PI3K inhibitors currently in the clinic induce global reprogramming of transcriptional and signaling pathways in tumor cells, paradoxically resulting in increased tumor cell motility and invasion. Mechanistically, this involves the trafficking of energetically active mitochondria to the cortical cytoskeleton of tumor cells, where they support membrane lamellipodia dynamics, turnover of FA complexes, and random cell migration and invasion. Conversely, interference with this spatiotemporal control of mitochondrial bioenergetics abolishes tumor cell invasion.

Although associated with important tumor traits, including "stemness" (20), malignant regrowth (21), and drug resistance (22), a general role of mitochondria in cancer has been difficult to determine (11). Whether these organelles play a role in tumor cell invasion and, therefore, metastatic competency has been equally controversial, with evidence that mitochondrial respiration is important (23), not important (24), or must be dysfunctional (25) to affect cell movements. Here disabling cellular respiration with depletion of mitochondrial DNA (26) or targeting an oxidative phosphorylation complex(es) (19) prevented mitochondrial trafficking to the cortical cytoskeleton, abolished membrane dynamics of cell motility, and suppressed cell invasion. Conversely, scavenging of mitochondrial ROS, which are increased in response to PI3K therapy, did not affect organelle dynamics and tumor cell invasion. Together, these data suggest that oxidative phosphorylation contributes to cancer metabolism and provides a "regional" and potent ATP source to fuel highly energy-demanding processes of cell movements and invasion (27).

This "spatiotemporal" model of mitochondrial bioenergetics is reminiscent of the accumulation of mitochondria at subcellular sites of energy-intensive processes in neurons (28), including synapses, active growth cones, and branches (29). Whether the cytoskeletal machinery that transports mitochondria along the microtubule network in neurons (30) is also exploited in cancer (this study) is currently unknown. However, there is evidence that comparable mechanisms of organelle dynamics (31) support mitochondrial redistribution in lymphocytes (32) and may contribute to directional migration of tumor cells (33). Consistent with this model (31), interference with the mitochondrial fusion machinery, namely mitofusins, suppressed mitochondrial

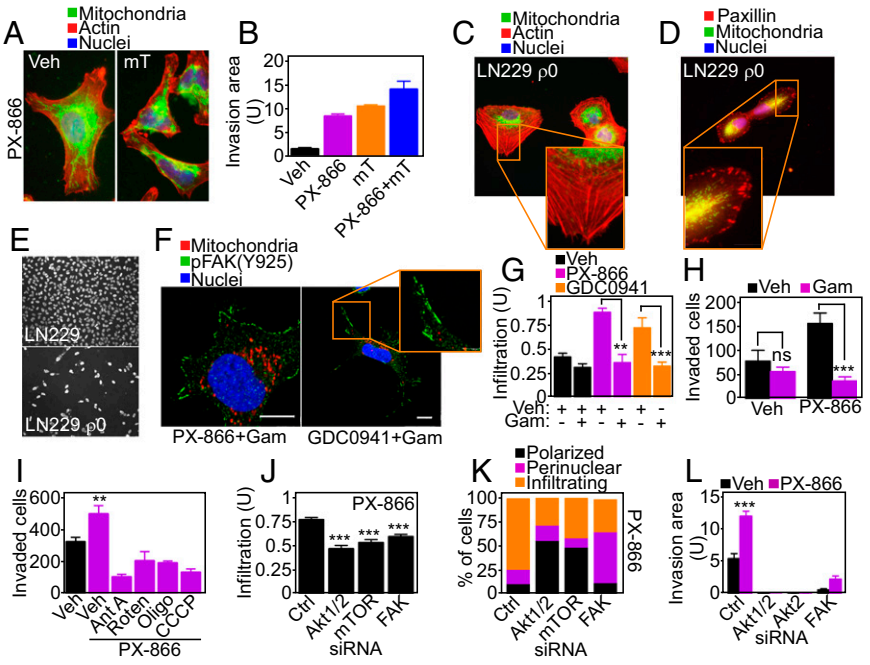

Fig. 4. Control of tumor cell invasion by spatiotemporal mitochondrial bioenergetics. (*A*) PC3 cells were labeled with MitoTracker Red, phalloidin Alexa488, and DAPI, treated with PX-866, and analyzed for mitochondrial infiltration into the peripheral cytoskeleton in the presence of vehicle or the mitochondrial-targeted ROS scavenger mitoTEMPO (mT; 50 μM). (*B*) PC3 cells were incubated with the indicated agents alone or in combination (PX-866+mT) and analyzed for tumor cell invasion across Matrigel. Mean ± SEM. *P* (ANOVA) < 0.0001. (*C* and *D*) Mitochondrial (mt)DNA-depleted LN229 (ρ0) cells were stimulated with NIH 3T3 conditioned media for 2 h, labeled with MitoTracker Red, DAPI, and either phalloidin Alexa488 (*C*) or an antibody to FA-associated paxillin (*D*), and analyzed by fluorescence microscopy. Representative pseudocolored images are shown. Magnification, 60×. (*E*) WT or ρ0 LN229 cells were analyzed for invasion across Matrigel-coated Transwell inserts. Representative images of invasive cells stained with DAPI are shown. Magnification, 20×. (*F*) PC3 cells treated with vehicle or PI3K inhibitors in combination with the mitochondrial-targeted small-molecule Hsp90 inhibitor Gamitrinib (Gam) were labeled with anti–pY925-FAK Alexa488 followed by fluorescence microscopy. Representative 1-μm extended-focus confocal images are shown. Magnification, 63×. (Scale bar, 10 μm.) (*G*) PC3 cells treated with vehicle or PI3K inhibitors with or without Gamitrinib (1 μM) were labeled with MitoTracker Red, phalloidin Alexa488, and DAPI and quantified after 48 h for mitochondrial infiltration into lamellipodia by fluorescence microscopy; $n = 48$. Mean ± SEM. $^{**}P = 0.0044$; $^{***}P < 0.0009$. (*H*) PC3 cells were treated with vehicle or PX-866 (5 μM) with or without Gamitrinib and quantified for invasion across Matrigel. Mean ± SEM of replicates ($n = 2$). $^{***}P < 0.0001$. ns, not significant. (*I*) PC3 cells were incubated with vehicle or PX-866 alone or in combination with the various mitochondrial respiratory chain inhibitors and analyzed for Matrigel invasion. Ant A, Antimycin A; Oligo, Oligomycin; Roten, Rotenone. Mean ± SEM. $^{**}P = 0.006$. (*J*) PC3 cells transfected with control siRNA or siRNA to Akt1/2, mTOR, or FAK were labeled as in *C*, treated with PX-866, and quantified for mitochondrial infiltration into lamellipodia; $n = 44$. Mean ± SEM. $^{***}P < 0.0001$. (*K*) siRNA-transfected PC3 cells labeled as in *C* were treated with PX-866 (5 μM) and analyzed for mitochondrial morphology (polarized, perinuclear, infiltrating) by fluorescence microscopy; $n = 21$. (*L*) PC3 cells transfected with the indicated siRNAs were quantified for invasion across Matrigel in the presence of vehicle or PX-866. Mean ± SEM ($n = 4$). $^{***}P < 0.0001$.

repositioning to the cortical cytoskeleton and tumor cell invasion mediated by PI3K therapy.

In addition to oxidative phosphorylation, Akt/mTOR signaling was identified here as a key regulator of mitochondrial trafficking and tumor cell invasion. This is consistent with a pivotal role of PI3K in directional cell movements (34), supporting chemotaxis at the leading edge of migration (35) and Rac1 activation (36). A third signaling requirement of this pathway involved FAK activity (18), which has also been implicated in cytoskeletal dynamics (37).

Despite hopes for "personalized" medicine (4), small-molecule PI3K inhibitors have produced modest and short-lived patient responses in the clinic (5). Our data suggest that these agents potently activate global adaptive mechanisms in tumors (7), unexpectedly centered on mitochondrial reprogramming in cell survival/bioenergetics (9) and subcellular trafficking (this study). In this context, the increased tumor cell motility and invasion stimulated by PI3K inhibitors may create an "escape" mechanism for tumor cells to elude therapy-induced environmental stress, reminiscent of the heightened metastatic propensity associated with other unfavorable conditions of hypoxia (38), acidosis (39), and antiangiogenic therapy (40, 41). Although this adaptive response to PI3K therapy may paradoxically promote more aggressive tumor traits and further compromise clinical outcomes, disabling mitochondrial adaptation is feasible (19) and may provide a viable strategy to increase the anticancer efficacy of PI3K antagonists in the clinic.

Methods

Two-Dimensional Chemotaxis. Cells were treated with PI3K inhibitors for 48 h and seeded in 2D chemotaxis chambers (Ibidi) in 10% (vol/vol) FBS medium. After a 6-h attachment, cells were washed and the reservoirs were filled with 0.1% BSA/RPMI, followed by gradient setup by addition of NIH 3T3 conditioned medium. Video microscopy was performed over 8 h, with a time-lapse interval of 10 min. At least 30 cells were tracked using the WimTaxis module (Wimasis), and the tracking data were exported into Chemotaxis and Migration Tool v2.0 (Ibidi) for graphing and statistical testing. Experiments were repeated twice ($n = 3$).

FA Dynamics. Cells growing in high–optical-quality 96-well μ-plates (Ibidi) were transduced with Talin-GFP BacMam virus (50 particles per cell) for 18 h and imaged with a 40× objective on a Nikon TE300 inverted time-lapse microscope equipped with a video system containing an Evolution QEi camera and a time-lapse video cassette recorder. The atmosphere was equilibrated to 37 °C and 5% CO_2 in an incubation chamber. Time-lapse fluorescence microscopy was carried out for the indicated times at 1 min per frame. Sequences were aligned in Image-Pro Plus 7 (Media Cybernetics) and imported into ImageJ (NIH) for further analysis. The initial and final frames were duplicated and assembled as composite images. FA complexes were manually counted and classified according to presence in some or all of the

time frames: decaying, newly formed, stable sliding (FA moves to a different position over time), and stable mature (merged areas). The rate of decay and assembly of FA complexes was calculated for each cell as the number of FA complexes changing per h. At least 400 FA complexes from 10 cells were analyzed from 5 independent time lapses per condition.

Tumor Cell Invasion. Experiments were carried out essentially as described (42). Briefly, 8-μm PET Transwell migration chambers (Corning) were coated with 150 μL 80 μg/mL Matrigel (Becton Dickinson). Tumor cells were seeded in duplicates onto the coated Transwell filters at a density of 1.25×10^5 cells per well in media containing 2% (vol/vol) FCS (FCIII; HyClone), and media containing 20% (vol/vol) FCS were placed in the lower chamber as chemoattractant. Cells were allowed to invade and adhere to the bottom of the plate, stained in 0.5% crystal violet/methanol for 10 min, rinsed in tap water, and analyzed by bright-field microscopy. Digital images were batch-imported into ImageJ, thresholded, and analyzed with the Analyze Particles function. For analysis of tumor cell invasion in 3D spheroids, tissue culture-treated 96-well plates were coated with 50 μL 1% Difco Agar Noble (Becton Dickinson). LN229 cells were seeded at 5,000 cells per well and allowed to form spheroids over 72 h. Spheroids were harvested, treated with PX-866 (0–10 μM), and placed in a collagen plug containing Eagle's minimum essential medium (EMEM), FBS, L-glutamine, sodium bicarbonate, and collagen type I (Gibco; 1.5 mg/mL). The collagen plug was allowed to set and 1 mL DMEM with 5% (vol/vol) FBS was added to the top of the plug. Cell invasion was analyzed every 24 h and quantified using Image-Pro Plus 7, as described (42).

Patient Samples. For studies using human samples, informed consent was obtained from all patients enrolled, and the study was approved by an Institutional Review Board of the Fondazione IRCCS Ca' Granda. The clinicopathological features of GBM patients used in this study are summarized in Table S1.

Statistical Analysis. Data were analyzed using either two-sided unpaired *t* test (for two-group comparisons) or one-way ANOVA test with Dunnett's multiple comparison posttest (for more than two-group comparisons) using a GraphPad software package (Prism 6.0) for Windows. Data are expressed as mean ± SD or mean ± SEM of multiple independent experiments. A *P* value of <0.05 was considered statistically significant.

ACKNOWLEDGMENTS. We thank James Hayden and Frederick Keeney of the Wistar Imaging Facility for outstanding help with time-lapse imaging. This work was supported by National Institutes of Health Grants P01 CA140043 (to D.C.A. and L.R.L.), R01 CA78810 and CA190027 (to D.C.A.), F32 CA177018 (to M.C.C.), and R01 CA089720 (to L.R.L.), the Office of the Assistant Secretary of Defense for Health Affairs through the Prostate Cancer Research Program under Award W81XWH-13-1-0193 (to D.C.A.), and a Joint Grant in Molecular Medicine 2013 from Fondazione IRCCS Ca' Granda and Istituto Nazionale Genetica Molecolare (to V.V.). Support for the core facilities used in this study was provided by Cancer Center Support Grant CA010815 to The Wistar Institute.

1. Engelman JA, Luo J, Cantley LC (2006) The evolution of phosphatidylinositol 3-kinases as regulators of growth and metabolism. *Nat Rev Genet* 7(8):606–619.
2. Manning BD, Cantley LC (2007) AKT/PKB signaling: Navigating downstream. *Cell* 129(7):1261–1274.
3. Vivanco I, Sawyers CL (2002) The phosphatidylinositol 3-kinase AKT pathway in human cancer. *Nat Rev Cancer* 2(7):489–501.
4. Rodon J, Dienstmann R, Serra V, Tabernero J (2013) Development of PI3K inhibitors: Lessons learned from early clinical trials. *Nat Rev Clin Oncol* 10(3):143–153.
5. Fruman DA, Rommel C (2014) PI3K and cancer: Lessons, challenges and opportunities. *Nat Rev Drug Discov* 13(2):140–156.
6. Jänne PA, Gray N, Settleman J (2009) Factors underlying sensitivity of cancers to small-molecule kinase inhibitors. *Nat Rev Drug Discov* 8(9):709–723.
7. Cohen AA, et al. (2008) Dynamic proteomics of individual cancer cells in response to a drug. *Science* 322(5907):1511–1516.
8. Chakrabarty A, Sánchez V, Kuba MG, Rinehart C, Arteaga CL (2012) Feedback upregulation of HER3 (ErbB3) expression and activity attenuates antitumor effect of PI3K inhibitors. *Proc Natl Acad Sci USA* 109(8):2718–2723.
9. Ghosh JC, et al. (2015) Adaptive mitochondrial reprogramming and resistance to PI3K therapy. *J Natl Cancer Inst* 107(3):dju502.
10. Ward PS, Thompson CB (2012) Metabolic reprogramming: A cancer hallmark even Warburg did not anticipate. *Cancer Cell* 21(3):297–308.
11. Wallace DC (2012) Mitochondria and cancer. *Nat Rev Cancer* 12(10):685–698.
12. Frezza C, et al. (2011) Haem oxygenase is synthetically lethal with the tumour suppressor fumarate hydratase. *Nature* 477(7363):225–228.
13. Vaira V, et al. (2010) Preclinical model of organotypic culture for pharmacodynamic profiling of human tumors. *Proc Natl Acad Sci USA* 107(18):8352–8356.
14. Roussos ET, Condeelis JS, Patsialou A (2011) Chemotaxis in cancer. *Nat Rev Cancer* 11(8):573–587.
15. Hinz B, Alt W, Johnen C, Herzog V, Kaiser H-W (1999) Quantifying lamella dynamics of cultured cells by SACED, a new computer-assisted motion analysis. *Exp Cell Res* 251(1):234–243.
16. Petrie RJ, Doyle AD, Yamada KM (2009) Random versus directionally persistent cell migration. *Nat Rev Mol Cell Biol* 10(8):538–549.
17. Youle RJ, van der Bliek AM (2012) Mitochondrial fission, fusion, and stress. *Science* 337(6098):1062–1065.
18. Sulzmaier FJ, Jean C, Schlaepfer DD (2014) FAK in cancer: Mechanistic findings and clinical applications. *Nat Rev Cancer* 14(9):598–610.
19. Chae YC, et al. (2013) Landscape of the mitochondrial Hsp90 metabolome in tumours. *Nat Commun* 4:2139.
20. Janiszewska M, et al. (2012) Imp2 controls oxidative phosphorylation and is crucial for preserving glioblastoma cancer stem cells. *Genes Dev* 26(17):1926–1944.
21. Viale A, et al. (2014) Oncogene ablation-resistant pancreatic cancer cells depend on mitochondrial function. *Nature* 514(7524):628–632.
22. Haq R, et al. (2013) Oncogenic BRAF regulates oxidative metabolism via PGC1α and MITF. *Cancer Cell* 23(3):302–315.
23. LeBleu VS, et al. (2014) PGC-1α mediates mitochondrial biogenesis and oxidative phosphorylation in cancer cells to promote metastasis. *Nat Cell Biol* 16(10):992–1003.
24. Shiraishi T, et al. (2015) Glycolysis is the primary bioenergetic pathway for cell motility and cytoskeletal remodeling in human prostate and breast cancer cells. Oncotarget 6(1):130–143.
25. Porporato PE, et al. (2014) A mitochondrial switch promotes tumor metastasis. *Cell Reports* 8(3):754–766.
26. Olgun A, Akman S (2007) Mitochondrial DNA-deficient models and aging. *Ann N Y Acad Sci* 1100:241–245.
27. De Bock K, et al. (2013) Role of PFKFB3-driven glycolysis in vessel sprouting. *Cell* 154(3):651–663.
28. Lee CW, Peng HB (2006) Mitochondrial clustering at the vertebrate neuromuscular junction during presynaptic differentiation. *J Neurobiol* 66(6):522–536.
29. Saxton WM, Hollenbeck PJ (2012) The axonal transport of mitochondria. *J Cell Sci* 125(Pt 9):2095–2104.
30. Birsa N, Norkett R, Higgs N, Lopez-Domenech G, Kittler JT (2013) Mitochondrial trafficking in neurons and the role of the Miro family of GTPase proteins. *Biochem Soc Trans* 41(6):1525–1531.
31. Zhao J, et al. (2013) Mitochondrial dynamics regulates migration and invasion of breast cancer cells. *Oncogene* 32(40):4814–4824.
32. Morlino G, et al. (2014) Miro-1 links mitochondria and microtubule dynein motors to control lymphocyte migration and polarity. *Mol Cell Biol* 34(8):1412–1426.
33. Desai SP, Bhatia SN, Toner M, Irimia D (2013) Mitochondrial localization and the persistent migration of epithelial cancer cells. *Biophys J* 104(9):2077–2088.
34. Kölsch V, Charest PG, Firtel RA (2008) The regulation of cell motility and chemotaxis by phospholipid signaling. *J Cell Sci* 121(Pt 5):551–559.
35. Weiger MC, et al. (2009) Spontaneous phosphoinositide 3-kinase signaling dynamics drive spreading and random migration of fibroblasts. *J Cell Sci* 122(Pt 3):313–323.
36. Kraynov VS, et al. (2000) Localized Rac activation dynamics visualized in living cells. *Science* 290(5490):333–337.
37. Fabry B, Klemm AH, Kienle S, Schäffer TE, Goldmann WH (2011) Focal adhesion kinase stabilizes the cytoskeleton. *Biophys J* 101(9):2131–2138.
38. Pennacchietti S, et al. (2003) Hypoxia promotes invasive growth by transcriptional activation of the met protooncogene. *Cancer Cell* 3(4):347–361.
39. Gatenby RA, Gillies RJ (2004) Why do cancers have high aerobic glycolysis? *Nat Rev Cancer* 4(11):891–899.
40. Ebos JM, et al. (2009) Accelerated metastasis after short-term treatment with a potent inhibitor of tumor angiogenesis. *Cancer Cell* 15(3):232–239.
41. Pàez-Ribes M, et al. (2009) Antiangiogenic therapy elicits malignant progression of tumors to increased local invasion and distant metastasis. *Cancer Cell* 15(3):220–231.
42. Caino MC, et al. (2013) Metabolic stress regulates cytoskeletal dynamics and metastasis of cancer cells. *J Clin Invest* 123(7):2907–2920.
43. Kang BH, et al. (2009) Combinatorial drug design targeting multiple cancer signaling networks controlled by mitochondrial Hsp90. *J Clin Invest* 119(3):454–464.
44. Ortensi B, et al. (2012) Rai is a new regulator of neural progenitor migration and glioblastoma invasion. *Stem Cells* 30(5):817–832.
45. Vaira V, et al. (2012) miR-296 regulation of a cell polarity-cell plasticity module controls tumor progression. *Oncogene* 31(1):27–38.
46. Livak KJ, Schmittgen TD (2001) Analysis of relative gene expression data using real-time quantitative PCR and the 2-ΔΔCT method. *Methods* 25(4):402–408.
47. Benjamini Y, Hochberg Y (1995) Controlling the false discovery rate: A practical and powerful approach to multiple testing. *J R Stat Soc Series B Stat Methodol* 57(1):289–300.
48. Louis DN, et al. (2007) The 2007 WHO classification of tumors of the central nervous system. *Acta Neurophatol* 114(2):97–109.